Ocean Sci. Discuss., doi:10.5194/os-2016-36, 2016
Manuscript under review for journal Ocean Sci.
Published: 14 June 2016

Ocean Science
Discussions
Open Access
EGU

Seasonal resonance of diurnal coastal trapped waves in the southern Weddell Sea, Antarctica

Stefanie Semper[1] and Elin Darelius[1,2]

[1]Geophysical Institute, University of Bergen, and Bjerknes Centre for Climate Research, Bergen, Norway
[2]Uni Research Climate, Bergen, Norway

Correspondence to: stefanie.semper@uib.no

Abstract.

The summer enhancement of diurnal tidal currents at the shelf break in the southern Weddell Sea is studied using velocity measurements from 29 moorings during the period 1968 to 2014. Kinetic energy associated with diurnal tidal frequencies is largest at the shelf break and decreases rapidly with distance; its magnitude increases from austral winter to summer by on average 50 %. The summer enhancement is observed in all deployments. The observations are compared to results from an idealised numerical solution of the properties of coastal trapped waves (CTWs) for a given bathymetry, stratification and an along-slope current. The frequency at which the dispersion curve for mode 1 CTWs displays a maximum (i.e. where the group velocity is zero and resonance is possible) is found within or near the diurnal frequency band, and it is sensitive to the stratification in the upper part of the water column and to the background current. The maximum of the dispersion curve is shifted towards higher frequencies, above the diurnal band, for low stratification and a strong background current (i.e. winter-like conditions) and towards lower frequencies for strong upper layer stratification and a weak background current (summer). The seasonal evolution of hydrography and currents in the region is inferred from available mooring data and conductivity-temperature-depth profiles. Near-resonance between CTWs and the diurnal tides during austral summer can explain the observed seasonality in tidal currents.

1 Introduction

The shelf break region in the southern Weddell Sea (Fig. 1) is an area of great climatic interest. This is where cold, dense Ice Shelf Water emerging from underneath the Filchner-Ronne Ice Shelf (FRIS) descends the continental slope (Foldvik et al., 2004), ultimately contributing to the formation of Antarctic Bottom Water which spreads out into the major oceans at abyssal depths (Orsi et al., 1999). Furthermore, warm off-shelf water crosses the shelf break during summer (Årthun et al., 2012) and flows southward towards the Filchner Ice shelf along the eastern flank of the Filchner Depression (Foldvik et al., 1985a, see map in Fig. 1 for location). The wind driven inflow of Modified Warm

Ocean Sci. Discuss., doi:10.5194/os-2016-36, 2016
Manuscript under review for journal Ocean Sci.
Published: 14 June 2016

Deep Water (MWDW) has been observed to reach the ice shelf front (Darelius et al., 2016), and climate models suggest a larger inflow and a dramatic increase in basal melt rates below the FRIS within the next century (Hellmer et al., 2012).

Physical processes at the shelf break and on the continental slope influence both the cold outflow and the warm inflow, and to some extent set their hydrographic properties and strengths. The variable depth of the thermocline, for example, which is controlled mainly by wind forcing and eddy overturning (Sverdrup, 1953; Nøst et al., 2011) will determine if and when warm water can access the continental shelf (Årthun et al., 2012). Meanwhile, it affects the density contrast between the cold outflow and the ambient water at the shelf break, and thus the strength of the geostrophically balanced outflow (Kida, 2011; Wang et al., 2012) as well as the properties of the descending dense plume (since it is a mixture of outflow water and ambient water, Darelius et al., 2014). The co-location of the critical latitude for the tidal component M2 and a critical slope leads to enhanced turbulence levels in the region (Fer et al., 2016). Mixing can be expected to be further enhanced at the shelf break by the strong diurnal tidal currents and the presence of continental shelf waves (Middleton et al., 1987; Foldvik et al., 1990; Jensen et al., 2013), a class of coastal trapped waves (CTWs). This study focusses on tidally generated CTWs at diurnal frequencies in the shelf-break region of the southern Weddell Sea.

Generally, CTWs can be generated by e.g. tides (Thomson and Crawford, 1982) or wind (Huthnance, 1995). Additionally, a connection between the generation of the waves and the outflow of dense shelf water through troughs has been suggested (Marques et al., 2014; Jensen et al., 2013). CTWs with sub-inertial frequencies propagate along a trapping boundary, e.g. a coastal wall or a sloping bottom (Huthnance, 1995; Huthnance et al., 1986). The waves require the support of such a boundary to exist and decay exponentially with increasing distance from it (Mysak, 1980). While CTWs propagate with shallow water to the left (in the southern hemisphere), the group velocity c_g, and thus the energy associated with the waves, can propagate in either direction. If the group velocity is zero, i.e. for a maximum in the dispersion curve of a wave, energy cannot propagate. When the frequency of this maximum (hereafter called "resonant frequency", RF) in the dispersion relation coincides with the frequency of tidal currents, resonance may occur and tidal currents will be amplified. In practice, it is likely that some energy can escape on one side along the shelf, resulting in near-resonance rather than resonance.

Such near-resonant diurnal CTWs were first recorded on the shelf of the Outer Hebrides of Scotland by Cartwright (1969) and have been observed and modelled at numerous occasions and locations since then (e.g. Huthnance, 1974; Crawford and Thomson, 1982; Heath, 1983; Hunkins, 1986; Padman et al., 1992; Skarðhamar et al., 2015). In our study region, Foldvik and Kvinge (1974) and Foldvik et al. (1985b) first suggested that CTWs caused the observed strong diurnal tidal currents, which broke down during winter presumably due to a seasonally varying stratification. Later, Middleton et al. (1987) and Foldvik et al. (1990) found a particularly strong enhancement of the K_1 tidal

Ocean Sci. Discuss., doi:10.5194/os-2016-36, 2016
Manuscript under review for journal Ocean Sci.
Published: 14 June 2016

constituent during austral summer. The summer maximum was hypothesised to be due to the interaction of barotropic CTWs with topography in the presence of a seasonally variable mean current (Foldvik et al., 1990). These studies were based on a small number of moorings and a barotropic shelf wave model neglecting the effects of stratification.

Our study is based on a more extensive data set and aims to provide new insight into the seasonal variability of the tidal currents at diurnal frequencies and its causes in the southern Weddell Sea. Observations of current velocities from 29 moorings are used to quantify the strength of diurnal tidal currents and to describe their spatial and temporal variability. We provide a novel description of the seasonal changes in shelf break hydrography based on observations and use a numerical code (Brink, 2006) in order to investigate the sensitivity of the CTW properties to seasonal changes in hydrography. The effects of the stratification and slope current on CTWs are compared, and the influences of the bathymetry and sea ice on CTWs are discussed.

2 Data and methods

Current meter data from 29 moorings (Foldvik et al., 2004; Jensen et al., 2013; Darelius et al., 2016) located on the continental slope and shelf in the area surrounding the Filchner Depression have been analysed. The records span the years 1968 to 2013 and are of 1–2 years duration. The locations of the moorings are shown in Fig. 1, and deployment details are listed in Table 1.

The coordinate system is rotated clockwise to align the y-axis with the isobaths, agreeing with the set-up of the numerical code (Brink, 2006) in the southern hemisphere. u is thus directed on-shelf and v along the continental slope (Fig. 1). The rotation angle β, positive for clockwise rotation, is listed in Table 1; it is inferred for each mooring from the local bathymetry based on the GEBCO_2014 bathymetry grid (The GEBCO_2014 Grid, version 20150318, http://www.gebco.net) with an estimated accuracy of approximately $\pm 10°$.

Time series of kinetic energy (KE) associated with the diurnal tidal currents are constructed as follows: The hourly-averaged current meter data are divided into chunks of 1.5 months length beginning every 14th day. For each chunk, the power spectral densities are estimated using Welch's method (Welch, 1976) and three 50 %-overlapping Hanning windows. The diurnal tidal KE is obtained by integrating the velocity spectra,

$$\mathrm{KE} = \int_{\omega_1}^{\omega_2} (S_u + S_v)\, d\omega, \tag{1}$$

where, following Jensen et al. (2013), ω_2 and ω_1 correspond to periods of 21.3 h and 26.9 h respectively.

Diurnal tidal KE has also been inferred using tidal predictions from the Circum-Antarctic Tidal Simulation (CATS, Padman et al., 2002) for the respective time and location of every mooring deployment. The tidal predictions are treated in the same way as the observational current velocities.

Ocean Sci. Discuss., doi:10.5194/os-2016-36, 2016
Manuscript under review for journal Ocean Sci.
Published: 14 June 2016

Tidal ellipses have been obtained from the mooring records using harmonic analysis (T_TIDE, Pawlowicz et al., 2002). When evaluating seasonal changes, the harmonic analysis was carried out on 50 % overlapping month-long segments of the records. The tidal constituent P_1 was then inferred from K_1 based on the year-long record, since the month-long segments are too short to separate the two signals.

Records of temperature and salinity from mooring M3, located at the 725 m isobath just upstream (i.e. to the east) of the Filchner outflow (Fig. 1), are used to describe the seasonal changes in hydrography at the shelf break and upper continental slope. The mooring records are complemented by a conductivity-temperature-depth (CTD) profile obtained during the deployment cruise in 2009 and by hydrographic measurements obtained in the vicinity of the M3 location (within 10 km, Fig. 1) provided by seals tagged with small CTD sensors (described in Årthun et al., 2012, hereafter referred to as "seal data"). The accuracies of the seals' temperature and salinity measurements are stated to be 0.005° C and 0.02, respectively (Boehme et al., 2009).

In addition, we use wind observations from Halley Research Station, located at 75° 35' S, 26° 39' W (Fig. 1), from 1957 to 2014 (British Antarctic Survey, 2013, updated 2014) and satellite derived records of sea ice concentration (Meier et al., 2013, updated 2015), available for the period 1978 to 2014. The sea ice concentration is averaged over the study area (inset in Fig. 1).

3 Observational results

3.1 Spatial and temporal variability of tidal currents

The diurnal tidal frequency band shows enhanced variance for both the u- and v-component, especially at the frequencies of the most important diurnal tidal constituents K_1 and O_1 (Fig. 2). High energy levels are additionally observed at semi-diurnal frequencies and around 35 h, as also found by Jensen et al. (2013).

The energy associated with the diurnal tidal currents, the diurnal tidal KE (Sect. 2), shows little variation with depth, except for a boundary layer at the bottom where diurnal tidal KE is slightly decreased compared to the overlying water column (Fig. 3). Depth-averaged diurnal tidal KE is used for further analysis.

Figure 4 shows the spatial distribution of diurnal tidal KE during austral summer. The magnitude of diurnal tidal KE is highest directly at the shelf break (e.g. moorings B2, F1, M3) and decreases rapidly with distance from it. The tidal currents rotate clockwise on the deeper continental slope and anticlockwise at the shelf break and on the shelf. The major axes of the tidal ellipses at the K_1 frequency are directed across the continental slope for moorings located at the shelf break and on the continental slope in the eastern part of the study area, while tidal currents recorded at moorings on the shelf are close to circular.

Ocean Sci. Discuss., doi:10.5194/os-2016-36, 2016
Manuscript under review for journal Ocean Sci.
Published: 14 June 2016

Time series of diurnal tidal KE (Fig. 5a) show two local maxima; one in austral summer and one in austral winter. These two peaks per year result from the interference of the diurnal tidal constituents K_1 and P_1, which are in phase every six months. The austral summer maximum is 30 % to 180 % higher than the winter maximum. This asymmetry is especially strong in records from moorings on the continental slope and at the shelf break, but it is observed in all deployments of sufficient length. For moorings on the continental shelf, the difference between the maxima is sometimes less pronounced (e.g. Fr2 in Fig. 5a). Minima of the diurnal tidal KE occur near the equinoxes in spring and autumn, when both the sun and the moon are close to the equator.

Time series of the K_1 magnitude obtained from harmonic analysis on monthly segments (see Section 2) show a seasonal signal with a maximum during austral summer which is apparent at all moorings (Fig. 5b) with the exception of F1, located at the 647 m isobath downstream of the Filchner outflow. F1 shows no increase in magnitude towards the end of the record when approaching austral summer. For all moorings, the semi-major axes are largest in the across-slope component u.

3.2 Seasonal variability of the hydrography and current on the upper slope

The seasonal variability in the hydrography at the shelf break and on the upper slope is investigated by merging all available observational data (moorings, CTD, seal data) near the location of mooring M3 (Fig. 6a,b). Cold and fresh Winter Water (WW) is found on top of warm and saline MWDW. MWDW is a mixture of WW and Warm Deep Water (WDW), the Weddell Sea version of the Circumpolar Deep Water which composes most part of the Antarctic Circumpolar Current.

While the temperature in the upper approximately 400 m is near the freezing point year-round, the salinity of the surface layer increases from 34.0 in February to 34.4 in October. The cold and fresh surface layer during summer likely results from local sea ice melt.

The thermocline is found at a depth of approximately 400 m from December to April and deepens by 200 m to approximately 600 m during May to August. Seasonal changes in the water column below the pycnocline are negligible. Generally, the seal data show higher salinities and temperatures at depth compared to the mooring data (also compared to the range of the unfiltered mooring records, not shown), suggesting that the MWDW and the thermocline are found higher up in the water column in 2011 compared to 2009.

The density profiles (Fig. 6c) show a gradual increase in density at the surface from $\sigma_0 \approx 27.3\,\mathrm{kg\,m^{-3}}$ to $27.7\,\mathrm{kg\,m^{-3}}$, indicating a relatively stable stratification in the upper part of the water column during austral summer and a relatively homogeneous, weakly stratified upper layer during austral winter.

Long-term observations of the westward flowing Antarctic slope current from this area are rare, and our knowledge of its strength, width and variability in our study region are limited. At 12° W, Fahrbach et al. (1992) observed a south-westward flowing current following the continental shelf break with annual mean velocities of 10–20 $\mathrm{cm\,s^{-1}}$ and a maximum velocity (hourly average) of

Ocean Sci. Discuss., doi:10.5194/os-2016-36, 2016
Manuscript under review for journal Ocean Sci.
Published: 14 June 2016

over 60 cm s^{-1}. Although inconclusive, the records suggest a wind-driven seasonal cycle with a magnitude of about 5 cm s^{-1} where maximum currents are observed in late autumn.

At 17° W, the core of the slope current is found above the 1000 m isobath with a surface velocity of 50 cm s^{-1} (Heywood et al., 1998). The current is suggested to weaken towards Halley Bay (Fahrbach et al., 1992). It splits at 27° W into two branches, one following the coast southwards and one continuing along the continental slope (Gill, 1973).

Mooring records from the region west of the Filchner Depression cover only the lower part of the water column, and the observations are greatly influenced by the Filchner overflow plume (Foldvik et al., 2004), thus giving little information about the slope current. East of the depression, the strongest along-slope currents are observed at mooring M3, relatively close to the shelf break at the 750 m isobath. Here, the monthly mean westward current reaches 17 cm s^{-1} during austral winter with maximum values of 25 cm s^{-1}. At mooring M4 (located at the 1050 m isobath, less than 10 km north of M3), no or very weak westward currents were observed.

4 Numerical code

4.1 Set-up

The numerical code described in Brink (2006) and adapted for the southern hemisphere by Jensen et al. (2013), is used to calculate the properties of stable, inviscid CTWs for different stratification, bathymetry and mean flow.

The code was set up using 30 vertical levels and 120 horizontal grid points to represent a 2 D-cross-slope section. Following Jensen et al. (2013), we use a closed coastal but open offshore boundary, a free surface and a negligible bottom friction as well as the bathymetry used in that study. The bathymetry represents an average of six across-slope sections in the area of moorings M1 to M5, and it compares well to sections farther west in our study area (not shown).

The input stratification vector (squared buoyancy frequency, N^2) is linearly interpolated onto the vertical levels of the code and duplicated for the horizontal cross-shelf section before it is converted to density, hence no across-shelf stratification changes are taken into account. If an along-shore current is specified, the background density field is altered by applying the thermal wind equation. The stratification used by the code is then determined from the density field by linear interpolation between the levels above and below each respective level of the code.

4.2 Sensitivity to stratification

A reference stratification profile was constructed based on all available CTD data collected in January and February in the eastern part of the study area. Similar profiles were constructed for areas farther to the west. Figure 7a shows the obtained density and stratification profiles, representative for the shelf break at the M-mooring array in austral summer. A simplified version of the stratification

Ocean Sci. Discuss., doi:10.5194/os-2016-36, 2016
Manuscript under review for journal Ocean Sci.
Published: 14 June 2016

profile (Fig. 7b) indicates the parameters changed in the sensitivity test: the strengths of the surface magnitude (SM) and the subsurface magnitude (SSM) around 500 m depth, the depth of the SSM (SSD) and the constant magnitude at depths below 1200 m ("deep magnitude", DM). The values of the applied parameter values are listed in Table 2.

The dispersion curves and their group velocities for wave modes 1 to 3 corresponding to the reference stratification (Fig. 7a) are presented in Fig. 8. Mode 1 is the only wave mode for which the dispersion curve shows a maximum, i.e. where the group velocity becomes zero. These results suggest that CTWs with a wavelength of approximately 1260 km and a period of approximately 30 h will be trapped while CTWs with tidal frequencies cannot exist. For tidal CTWs to exist, the dispersion curve must pass through the tidal band, i.e. the RF must lie within (thus giving near-resonance) or above the diurnal tidal frequency band.

As the numerical code has a vertical resolution of 160 m, defining the uppermost N^2 value is not a straightforward task. For the reference stratification profile (Fig. 7), the surface N^2 value used in the numerical code is from 20 m depth. Using the surface profile value or an average of the upper 80 m shifts the dispersion curves and thus the RF to higher frequencies (Fig. 8). For stratification profiles which are representative for areas farther west at the shelf break and constructed similarly to the reference stratification with surface N^2 values of the upper 80 m average, the dispersion curve and RF are similarly shifted to higher frequencies (Fig. 8).

Keeping in mind the variations along the shelf break and with different approaches on how to choose the uppermost stratification value, the characteristic parameters of the reference profile (SM, SSM, SSD, DM, Fig. 7b) are varied in the following to explore the general effects of stratification on the dispersion curve and the RF.

Figure 9 shows the results from the sensitivity test for stratification, where the RF is identified from each dispersion curve obtained from the modified stratification input. An increase of N^2 at the surface (case SM) leads to a decrease in RF, which moves through the diurnal tidal frequency band for the modelled range of surface stratification. Contrarily to case SM, an increase of the stratification maximum at approximately 640 m depth (case SSM) increases the RF. The effect of an increase in depth of the subsurface maximum (case SSD) results in an apparent decrease of the RF. However, due to the interpolation in the numerical code, the stratification around the subsurface maximum as well as the exact value of the maximum are difficult to preserve. Hence, the actual effect of case SSD appears to be rather small. Varying the stratification below 1200 m depth (case DM) has a negligible effect on the RF.

4.3 Sensitivity to along-slope current

The optional along-shore current has a Gaussian shape; its offshore, onshore, upward and downward e-folding length scales must be specified, in addition to the centre position, strength and depth of the current.

Ocean Sci. Discuss., doi:10.5194/os-2016-36, 2016
Manuscript under review for journal Ocean Sci.
Published: 14 June 2016

For the sensitivity test, a barotropic (i.e. with a large vertical length scale) westward current is assumed which is centred at the shelf break. The density is set to be undisturbed at the coast when the density field is altered according to the thermal wind equation, with the input N^2 vector being the reference stratification for all runs. The width and strength of the current are varied from 10 to 100 km and 0.1 to 0.5 m s^{-1}, respectively (Fig. 10). Generally, both a stronger and a wider current lead to an increase in RF; with the effect of strength being largest.

Moving the location of the current core 40 km on (off) shore, the sensitivity of the RF is increased (reduced) slightly compared to a current core at the shelf break. The magnitude of change in RF equals approximately a change in current velocity of ± 10 cm s^{-1} (not shown).

Although the overall effect of an added barotropic slope current is minor compared to the sensitivity to changes in stratification (cp. y-axes in Fig. 9 and Fig. 10), the sensitivity depends noticeably on the vertical length scale. As an example, a 40 km wide and 0.2 m s^{-1} fast current is chosen and its downward e-folding length scale is reduced from 4300 m to 2000 m. The RF is then considerably larger (open circle in Fig. 10) than for the more barotropic case.

5 Discussion

Observations from the continental slope in the southern Weddell Sea show anomalously strong tidal currents at diurnal frequencies (Middleton et al., 1987). Our extended analysis - including all current meter records (1968–2014) from the region - confirms previous findings suggesting that the strong currents are the result of tidally forced CTWs (Middleton et al., 1987; Foldvik et al., 1990, 1985b). The observations agree qualitatively with the mode 1 CTW "generated" in the numerical code by Brink (2006), Fig. 11; notably the direction of rotation changes at the slope, and the strength of the currents increases towards the shelf break, as expected. The dispersion relation obtained from the model when using bathymetry and stratification representative for the region (Fig. 8) suggests that diurnal CTWs may be near-resonant, i.e. that the group velocity is zero or close to zero so that energy cannot propagate out of the area resulting in amplified diurnal tidal currents. A similar result was obtained by Middleton et al. (1987) using a barotropic shelf wave model (Saint-Guily, 1976). Tidal currents may be enhanced for a range of frequencies surrounding the RF, and thus RF does not need to coincide with a tidal frequency for amplification to occur (Chapman, 1989).

The dispersion curves in Fig. 8 show that while the CTWs are relatively barotropic in the region (according to the Burger number, $Bu = \left(\frac{NH}{fL}\right)^2$, $Bu \ll 1$, where N^2 is stratification, f the Coriolis factor and H and L are representative depth and length scales, respectively; Wang and Mooers, 1976; Brink, 2006; Jensen et al., 2013), the dispersion curve is sensitive to relatively small changes in the stratification.

Time series of the KE associated with the diurnal tides and of the tidal amplitudes derived by harmonic analysis show that diurnal tidal currents consistently are enhanced by 30–180 % during

Ocean Sci. Discuss., doi:10.5194/os-2016-36, 2016
Manuscript under review for journal Ocean Sci.
Published: 14 June 2016

austral summer. The astronomical diurnal tidal forcing and its seasonal variability cannot explain the asymmetry of the maxima in diurnal tidal KE. Studying a small subset of the moorings, Foldvik et al. (1985b) hypothesised that changing stratification causes the breakdown of the diurnal tidal currents observed during austral winter of 1968, while Foldvik et al. (1990) suggested that the seasonality was linked to the variability of the slope current. Other potential explanations are seasonal changes in the sea ice cover, as high sea ice concentrations would potentially dampen the CTWs (Ono et al., 2008), or in wind forcing, which could potentially excite CTWs (Gordon and Huthnance, 1987) at diurnal frequencies. These influences will be discussed below.

Hydrography and currents, which are known to vary seasonally, will alter the properties of the CTWs (e.g. Marques et al., 2014; Jensen et al., 2013; Brink, 1991; Wang and Mooers, 1976). We hypothesise that the observed seasonality in the diurnal tidal currents is indirectly linked to seasonal changes in the oceanographic "background", as it determines the dispersion relation including the RF for the CTWs which are responsible for the tidal amplification in the area.

The largest seasonal changes in the shelf break hydrography in the region occurs, similar to regions farther east in the Weddell Sea (Nøst et al., 2011; Graham et al., 2013), above the pycnocline. Cooling and a gradual increase in salinity (due to ice freezing and brine rejection) during austral autumn and winter leads to a gradual deepening of the surface layer. Towards the end of the winter (August–September) the upper 400 m are relatively homogeneous. During summer, the winter layer is capped by a fresh and relatively warm surface layer which likely is the result of local sea-ice melt and solar heating. The layer of summer surface water is thin (10-100 m, see CTD-profile in Fig. 6) and greatly increases the stratification by creating a seasonal, shallow pycnocline. The sensitivity test (Fig. 9) shows that the value of the RF is sensitive to the stratification in the upper layer (SM) and that it increases for decreasing stratification. The response in RF to realistic changes in SM is of sufficient magnitude to cause the RF to move through the diurnal tidal band.

While the RF is influenced by changes in the strength of the permanent (deeper) pycnocline (SSM), which is the manifestation of the transition from WW above to MWDW and WDW below, there is no observational evidence suggesting that it would change in magnitude. The depth of the permanent pycnocline (SSD), however, increases from about 400 m in summer to about 600 m, but changes in SSD have little or no influence on the RF.

Foldvik et al. (1990) showed how changes in the background current will affect the phase of diurnal CTWs, which are assumed to be generated upstream, as they arrive in the study region. Here we have investigated, similar to the work by Skarðhamar et al. (2015), the effect of changes in the background current on the dispersion relation and hence on the possibility for local near-resonance.

The available observations do not allow us to describe either the nature or the variability of the slope current, but the data from mooring M3 suggest that, in agreement with observations upstream (Nøst et al., 2011; Graham et al., 2013; Núñez-Riboni and Fahrbach, 2009), the westward flowing slope current is intensified during austral winter. When a barotropic, westward background current

Ocean Sci. Discuss., doi:10.5194/os-2016-36, 2016
Manuscript under review for journal Ocean Sci.
Published: 14 June 2016

is included in our set-up, the dispersion curve (and thus the RF) is shifted toward higher frequencies (Fig. 10 and Jensen et al., 2013), but the effect is small compared to the effect of stratification changes. The stronger current observed during austral autumn and winter will however add to the effect of the low winter time stratification and move the RF upwards.

While the tidal force is the main generation mechanism for CTWs in the diurnal tidal band (Thomson and Crawford, 1982), CTWs can also be generated by winds (Huthnance et al., 1986). Short duration storms have been observed to excite near-resonant CTWs of mode 1 (Gordon and Huthnance, 1987), i.e. the response to storms would in our case resemble the tidally forced waves. Time series of wind from the nearby Halley Research Station (see Fig. 1 for location), however, show that storms (wind speed $>20\,\mathrm{m\,s^{-1}}$) are rare during austral summer and, as expected, more frequent during winter and early spring. CTWs induced by storms can hence not explain the summer enhancement of the diurnal tidal currents. Fourier analysis of the time series reveals a daily cycle in wind strength with an increase of magnitude of up to $1.4\,\mathrm{m\,s^{-1}}$ around noon, which likely results from local boundary layer effects: The stable boundary layer which develops during the night is destroyed during the day by mixing due to solar insolation (see, e.g. Stull, 2012). Since the signal is weak, we conclude that these oscillations are not responsible for the observed summer amplification.

The study region is fully or partly covered by sea ice throughout the year, with the coverage normally exceeding 90 % during winter (mid-April to mid-November) and decreasing to a minimum of on average 50 % in February with considerable spatial differences within the study region (Fig. 13). Frictional damping of tidal CTWs due to sea ice is suggested to be the cause of the observed reduction of tidal currents over the shelf in the Sea of Okhotsk (Ono et al., 2008). The damping is observed only at the mooring farthest away from the generation site of the waves, indicating an increasing effect of the damping with distance. The authors do not explain why the period with reduced tides are much shorter (and misaligned) compared to the period with dense (>80 %) sea ice cover. While we can neither quantify nor rule out the effect of sea ice concentration, we note that the semi-diurnal tidal currents are observed to be larger during austral winter than during summer (Foldvik et al., 1990), thus questioning a general damping effect.

Skarðhamar et al. (2015) studied diurnal tides on the Barents Sea continental slope in a 3 D-model and concluded that the tidally generated CTWs were confined to a region with diverging bathymetry. Just east of our study region, the continental slope is much steeper (Fig. 1), that is, the isobaths diverge towards the west. The dispersion curve obtained using the steeper, eastward bathymetry is shifted upward with respect to the gentler slope in the study region (Fig. 8). Tidal energy travelling westward along the steep, eastern part of the slope could potentially be "piling up" in the more gently sloping study region where westward propagation no longer is possible. Above the steep, eastern slope, there are no direct observations of tidal currents, but the tidal motion of sea ice above the shelf break there suggests much weaker currents (Padman and Kottmeier, 2000). A full

Ocean Sci. Discuss., doi:10.5194/os-2016-36, 2016
Manuscript under review for journal Ocean Sci.
Published: 14 June 2016

3 D-analysis, similar to the one by Skarðhamar et al. (2015), would be needed to fully explore the effect of bathymetry.

The anomalously large diurnal tidal currents and the CTWs will influence e.g. the ice cover (Padman et al., 2002), and, potentially, the exchange of WDW across the shelf break. In an idealised model study, CTWs were shown to enhance the inflow of warm water through a trough cross-cutting the continental shelf (St-Laurent et al., 2013), similar to the Filchner Depression. We note that the depth of the WW–WDW transition (identified e.g. by the -1° C isotherm) varies on diurnal time scales (Fig. 12a), and e.g. in December 2009, the vertical excursion of the isotherm associated with the diurnal tides is >100 m (Fig. 12b). The depth of the transition is likewise affected by CTWs with 35 h period (Fig. 12a, Jensen et al., 2013). The existence and strength of diurnal (and longer period, Jensen et al., 2013) CTWs in the region must hence be expected to directly influence the availability of warm water above the shelf depth, i.e. at depths where it can potentially access the continental shelf. Furthermore, it was recently shown that elevated turbulence levels in the shelf-break region are linked to the semi-diurnal tide and the co-location of critical slope and critical latitude (Fer et al., 2016). The tides thus influence the water mass properties (through mixing) as well as the strength and depth of the thermocline at the shelf break. Modelling efforts aiming to describe and predict the oceanic heat transport towards the FRIS cavity inflow thus ought to include tidal forcing to correctly capture the dynamics at the shelf break.

Finally, we mention that the observed diurnal tidal currents are up to one order of magnitude larger than those predicted by the tidal model CATS (Fig. 11, Padman et al., 2002), and that the predictions from CATS do not reveal the summer enhancement. Moreover, due to errors in the model bathymetry, the predicted peak tidal currents are not consistently aligned with the shelf break when running CATS along a cross-shelf section through the locations of moorings M1 and M2 (see Fig. 11 and Fig. 1 for location of section). Hence, care must be taken when using CATS to de-tide velocity observations from the region.

6 Conclusions

Velocity measurements at 29 moorings located on the continental slope and shelf in the southern Weddell Sea from the period 1968 to 2014 show pronounced diurnal tidal variability. Diurnal tidal currents are strongest at the shelf break and substantially enhanced during austral summer. The summer enhancement is not predicted by the tidal model CATS (Padman et al., 2002). We investigated the possibility for near-resonant CTWs causing the enhanced diurnal tidal currents by using a 2 D-numerical code to obtain CTW properties (Brink, 2006). Dispersion curves of mode 1 CTWs have a maximum in frequency (the RF), which results in zero group velocity, i.e. trapped energy. The RF moves in and out of the diurnal tidal frequency band depending on the stratification and the slope current which both vary seasonally as hydrographic and current observations at the shelf break re-

Ocean Sci. Discuss., doi:10.5194/os-2016-36, 2016
Manuscript under review for journal Ocean Sci.
Published: 14 June 2016

veal. For the weakly stratified water column and strong slope current during austral winter, the RF is found above the diurnal band, suggesting the generation of weak, non-resonant tidal CTWs which quickly propagate out of the generation area. For austral summer conditions, i.e. a more stratified upper water column combined with a weaker slope current, the RF can fall into the diurnal band, thus leading to near-resonant diurnal CTWs enhancing the tidal currents. While no direct influence of wind on the diurnal tidal currents has been found, the varying bathymetry east of the study area as well as the sea ice cover likely affect the propagation of the CTWs. Further studies, using 3 D-models for example, are needed to quantify these influences as well as to detect the generation site of the CTWs. The shelf break region in the southern Weddell Sea is an area of great climatic interest. Cold, dense Ice Shelf Water descends the continental slope and contributes eventually to the formation of Antarctic Bottom Water, while warm MWDW flowing onto the shelf prospectively may reach the cavity below FRIS, thus enhancing basal melt rates. The strong diurnal tidal currents at the shelf break facilitate the cross-shelf exchange of water masses and contribute to mixing, hence influencing the hydrographic properties of both the cold outflow and warm inflow.

Acknowledgements. For deployment and recovery of moorings, we would like to thank AWI and the crew and scientists on RV *Polarstern* cruises PS08 (recovery of moorings D1, D2, S2-1985 and S3), PS12 (deployment S2-1987), PS34 (deployment Fr1 and Fr2), PS53 (recovery F1–4) and PS82 (recovery SB, SC, SD and SE). We would also like to thank K. Brink for sharing the numerical code and I. Fer for helpful comments and suggestions. The research was partially funded by the Centre for Climate Dynamics at the Bjerknes Centre.

Ocean Sci. Discuss., doi:10.5194/os-2016-36, 2016
Manuscript under review for journal Ocean Sci.
Published: 14 June 2016

References

Årthun, M., Nicholls, K. W., Makinson, K., Fedak, M. A., and Boehme, L.: Seasonal inflow of warm water onto the southern Weddell Sea continental shelf, Antarctica, Geophysical Research Letters, 39, doi:10.1029/2012GL052856, http://doi.wiley.com/10.1029/2012GL052856, 2012.

Boehme, L., Lovell, P., Biuw, M., Roquet, F., Nicholson, J., Thorpe, S. E., Meredith, M. P., and Fedak, M.: Technical Note: Animal-borne CTD-Satellite Relay Data Loggers for real-time oceanographic data collection, Ocean Sci., 5, 685–695, doi:10.5194/os-5-685-2009, 2009.

Brink, K. H.: Coastal-trapped waves and wind-driven currents over the continental shelf, Annu. Rev. Fluid Mech., 23, 389–412, doi:10.1146/annurev.fl.23.010191.002133, 1991.

Brink, K. H.: Coastal-Trapped Waves with Finite Bottom Friction, Dyn. Atmos. Oceans, 41, 172–190, doi:10.1016/j.dynatmoce.2006.05.001, 2006.

British Antarctic Survey: UK Antarctic Surface Meteorology; 1947–2013, Database, Version 1.0, Polar Data Centre, British Antarctic Survey, http://dx.doi.org/10.5285/569d53fb-9b90-47a6-b3ca-26306e696706, 2013, updated 2014.

Cartwright, D. E.: Extraordinary Tidal Currents near St Kilda, Nature, 223, 928–932, doi:10.1038/223928a0, 1969.

Chapman, D. C.: Enhanced subinertial diurnal tides over isolated topographic features, Deep Sea Research Part A. Oceanographic Research Papers, 36, 815–824, doi:10.1016/0198-0149(89)90030-7, http://linkinghub.elsevier.com/retrieve/pii/0198014989900307, 1989.

Crawford, W. and Thomson, R.: Continental Shelf Waves of Diurnal Period Along Vancouver Island, Journal of Geophysical Research, 87, 9516–9522, http://onlinelibrary.wiley.com/doi/10.1029/JC087iC12p09516/full, 1982.

Darelius, E., Makinson, K., Daae, K., Fer, I., Holland, P. R., and Nicholls, K. W.: Circulation and hydrography in the Filchner Depression, Journal of Geophyscial Research, 119, doi:10.1002/2014JC010225, 2014.

Darelius, E., Fer, I., and Nicholls, K. W.: Observed vulnerability of Filchner-Ronne Ice Shelf to wind-driven inflow of warm deep water, Nature communications, in review, 2016.

Fahrbach, E., Rohardt, G., and Krause, G.: The Antarctic Coastal Current in the southeastern Weddell Sea, Polar Biology, 12, 171–182, doi:10.1007/BF00238257, http://link.springer.com/10.1007/BF00238257, 1992.

Fer, I., Darelius, E., and Daae, K. B.: Observations of energetic turbulence on the Weddell Sea continental slope, Geophysical Research Letters, pp. 760–766, doi:10.1002/2015GL067349, http://dx.doi.org/10.1002/2015GL067349, 2015GL067349, 2016.

Foldvik, A. and Kvinge, T.: Bottom Currents in the Weddell Sea, Geophysical Institute Rep. No. 37, University of Bergen, 1974.

Foldvik, A., Gammelsrød, T., and Tørresen, T.: Circulation and water masses on the southern Weddell Sea shelf, Antarctic Research Series, 43, 5–20, doi:10.1029/AR043p0005, 1985a.

Foldvik, A., Kvinge, T., and Tørresen, T.: Bottom currents near the continental shelf break in the Weddell Sea, Oceanology of the Antarctic Continental Shelf, 43, doi:10.1029/AR043p0021, 1985b.

Foldvik, A., Middleton, J. H., and Foster, T. D.: The tides of the southern Weddell Sea, Deep Sea Research Part A. Oceanographic Research Papers, 37, 1345–1362, doi:10.1016/0198-0149(90)90047-Y, http://linkinghub.elsevier.com/retrieve/pii/019801499090047Y, 1990.

Ocean Sci. Discuss., doi:10.5194/os-2016-36, 2016
Manuscript under review for journal Ocean Sci.
Published: 14 June 2016

Foldvik, A., Gammelsrød, T., Østerhus, S., Fahrbach, E., Rohardt, G., Schröder, M., Nicholls, K. W., Padman, L., and Woodgate, R. A.: Ice shelf water overflow and bottom water formation in the southern Weddell Sea, Journal of Geophysical Research, 109, doi:10.1029/2003JC002008, http://doi.wiley.com/10.1029/2003JC002008http://onlinelibrary.wiley.com/doi/10.1029/2003JC002008/full, 2004.

Gill, A. E.: Circulation and bottom water production in the Weddell Sea, Deep-Sea Research, 20, 111–140, doi:10.1016/0011-7471(73)90048-X, 1973.

Gordon, R. L. and Huthnance, J. M.: Storm-driven continental shelf waves over the Scottish continental shelf, Continental Shelf Research, 7, 1015–1048, doi:10.1016/0278-4343(87)90097-5, http://linkinghub.elsevier.com/retrieve/pii/0278434387900975, 1987.

Graham, J. A., Heywood, K. J., Chavanne, C. P., and Holland, P. R.: Seasonal variability of water masses and transport on the Antarctic continental shelf and slope in the southeastern Weddell Sea, Journal of Geophysical Research: Oceans, 118, 2201–2214, doi:10.1002/jgrc.20174, http://doi.wiley.com/10.1002/jgrc.20174, 2013.

Heath, R. A.: Tidal currents in the southwestern Pacific Basin and Campbell Plateau, southeast of New Zealand, Deep Sea Research Part A. Oceanographic Research Papers, 30, 393–409, doi:10.1016/0198-0149(83)90074-2, http://linkinghub.elsevier.com/retrieve/pii/0198014983900742, 1983.

Hellmer, H. H., Kauker, F., Timmermann, R., Determann, J., and Rae, J.: Twenty-first-century warming of a large Antarctic ice-shelf cavity by a redirected coastal current, Nature, 485, 225–228, doi:10.1038/nature11064, http://www.nature.com/nature/journal/v485/n7397/abs/nature11064.html, 2012.

Heywood, K. J., Locarnini, R. A., Frew, R. D., Dennis, P. F., and King, B. A.: Transport and water masses of the Antarctic Slope Front system in the eastern Weddell Sea, Ocean, ice, and atmosphere: Interactions at the Antarctic continental margin, Antarctic Research Series, 75, 203–214, http://onlinelibrary.wiley.com/doi/10.1029/AR075p0203/summary, 1998.

Hunkins, K.: Anomalous diurnal tidal currents on the Yermak Plateau, Journal of Marine Research, 44, 51–69, doi:10.1357/002224086788460139, http://openurl.ingenta.com/content/xref?genre=article&issn=0022-2402&volume=44&issue=1&spage=51, 1986.

Huthnance, J. M.: On the diurnal tidal currents over Rockall Bank, Deep Sea Research, 21, 23–35, doi:10.1016/0011-7471(74)90016-3, 1974.

Huthnance, J. M.: Circulation, exchange and water masses at the ocean margin: the role of physical processes at the shelf edge, Progress in Oceanography, 35, 353–431, doi:10.1016/0079-6611(95)80003-C, 1995.

Huthnance, J. M., Mysak, L. A., and Wang, D.-P.: Coastal trapped waves, in: Baroclinic Processes on Continental Shelves, edited by Mooers, C. N., vol. 3, American Geophysical Union, Washington, D. C., doi:10.1029/CO003p0001, 1986.

Jensen, M. F., Fer, I., and Darelius, E.: Low frequency variability on the continental slope of the southern Weddell Sea, Journal of Geophysical Research: Oceans, 118, 1–17, doi:10.1002/jgrc.20309, http://doi.wiley.com/10.1002/jgrc.20309, 2013.

Kida, S.: The Impact of Open Oceanic Processes on the Antarctic Bottom Water Outflows, Journal of Physical Oceanography, 41, 1941–1957, doi:10.1175/2011JPO4571.1, 2011.

Marques, G. M., Padman, L., Springer, S. R., Howard, S. L., and Özgökmen, T. M.: Topographic vorticity waves forced by Antarctic dense shelf water outflows, Geophysical Research Letters, 41, 1247–1254, doi:10.1002/2013GL059153, http://doi.wiley.com/10.1002/2013GL059153, 2014.

Ocean Sci. Discuss., doi:10.5194/os-2016-36, 2016
Manuscript under review for journal Ocean Sci.
Published: 14 June 2016

Meier, W., Fetterer, F., Savoie, M., Mallory, S., Duerr, R., and Stroeve, J.: NOAA/NSIDC Climate Data Record of Passive Microwave Sea Ice Concentration, Version 2, http://dx.doi.org/10.7265/N55M63M1, Boulder, Colorado USA. NSIDC: National Snow and Ice Data Center. Date accessed: 15/11/2016, 2013, updated 2015.

Middleton, J. H., Foster, T. D., and Foldvik, A.: Diurnal Shelf Waves in the Southern Weddell Sea, Journal of Physical Oceanography, 17, 784 – 791, http://dx.doi.org/10.1175/1520-0485(1987)017<0784:DSWITS>2.0.CO;2, 1987.

Mysak, L. A.: Recent Advances in Shelf Wave Dynamics, Reviews of Geophysics and Space Physics, 18, 211–241, doi:10.1029/RG018i001p00211, 1980.

Nøst, O. A., Biuw, M., Tverberg, V., Lydersen, C., Hattermann, T., Zhou, Q., Smedsrud, L. H., and Kovacs, K. M.: Eddy overturning of the Antarctic Slope Front controls glacial melting in the Eastern Weddell Sea, Journal of Geophysical Research, 116, doi:10.1029/2011JC006965, http://doi.wiley.com/10.1029/2011JC006965, 2011.

Núñez-Riboni, I. and Fahrbach, E.: Seasonal variability of the Antarctic Coastal Current and its driving mechanisms in the Weddell Sea, Deep Sea Research Part I: Oceanographic Research Papers, 56, 1927–1941, doi:10.1016/j.dsr.2009.06.005, http://linkinghub.elsevier.com/retrieve/pii/S0967063709001344, 2009.

Ono, J., Ohshima, K. I., Mizuta, G., Fukamachi, Y., and Wakatsuchi, M.: Diurnal coastal-trapped waves on the eastern shelf of Sakhalin in the Sea of Okhotsk and their modification by sea ice, 28, 697–709, doi:10.1016/j.csr.2007.11.008, 2008.

Orsi, A. H., Johnson, G. C., and Bullister, J. L.: Circulation, mixing, and production of Antarctic Bottom Water, Progress in Oceanography, 43, 55–109, doi:10.1016/S0079-6611(99)00004-X, 1999.

Padman, L. and Kottmeier, C.: High-frequency ice motion and divergence in the Weddell Sea, Journal of Geophysical Research, 105, 3379–3400, doi:10.1029/1999JC900267, 2000.

Padman, L., Plueddemann, A. J., Muench, R. D., and Pinkel, R.: Diurnal tides near the Yermak Plateau, Journal of Geophysical Research, 97, 12 639–12 652, doi:10.1029/92JC01097, 1992.

Padman, L., Fricker, H. A., Coleman, R., Howard, S., and Erofeeva, L.: A new tide model for the Antarctic ice shelves and seas, Annals of Glaciology, 34, 247–254, doi:10.3189/172756402781817752, 2002.

Pawlowicz, R., Beardsley, B., and Lentz, S.: Classical tidal harmonic analysis including error estimates in MATLAB using T_TIDE, Computers & Geosciences, 28, 929–937, doi:10.1016/S0098-3004(02)00013-4, http://linkinghub.elsevier.com/retrieve/pii/S0098300402000134, 2002.

Saint-Guily, B.: Sur la propagation des ondes de seconde classe le long d'un talus continental, C. R. Acad. Sci. Paris, 282, 1976.

Skarðhamar, J., Skagseth, Ø., and Albretsen, J.: Diurnal tides on the Barents Sea continental slope, Deep Sea Research I, 97, 40–51, doi:10.1016/j.dsr.2014.11.008, http://linkinghub.elsevier.com/retrieve/pii/S096706371400212X, 2015.

St-Laurent, P., Klinck, J. M., and Dinnimann, M. S.: On the Role of Coastal Troughs in the Circulation of Warm Circumpolar Deep Water on Antarctic Shelves, Journal of Physical Oceanography, 43, 51–64, doi:10.1175/JPO-D-11-0237.1, 2013.

Stull, R. B.: An introduction to boundary layer meteorology, vol. 13, Springer Science & Business Media, doi:10.1007/978-94-009-3027-8, 2012.

Ocean Sci. Discuss., doi:10.5194/os-2016-36, 2016
Manuscript under review for journal Ocean Sci.
Published: 14 June 2016

Sverdrup, H. U.: The currents off the coast of Queen Maud Land, Særtrykk av Norsk Geografisk Tidsskrift, 14, 239–249, doi:10.1080/00291955308551737, 1953.

Thomson, R. E. and Crawford, W. R.: The Generation of Diurnal Period Shelf Waves by Tidal Currents, Journal of Physical Oceanography, 12, 635–643, http://dx.doi.org/10.1175/1520-0485(1982)012<0635:TGODPS>2.0.CO;2, 1982.

Wang, D.-P. and Mooers, C. N.: Coastal-Trapped Waves in a Continuously Stratified Ocean, Journal of Physical Oceanography, 6, 853 – 863, http://dx.doi.org/10.1175/1520-0485(1976)006<0853:CTWIAC>2.0.CO;2, 1976.

Wang, Q., Danilov, S., Fahrbach, E., Schröter, J., and Jung, T.: On the impact of wind forcing on the seasonal variability of Weddell Sea Bottom Water transport, Geophysical Research Letters, 39, doi:10.1029/2012GL051198, 2012.

Welch, P. D.: The use of fast Fourier transform for the estimation of power spectra: a method based on time averaging over short, modified periodograms, IEEE Transactions on Audio and Electroacoustics, 2, 70–73, 1976.

Ocean Sci. Discuss., doi:10.5194/os-2016-36, 2016
Manuscript under review for journal Ocean Sci.
Published: 14 June 2016

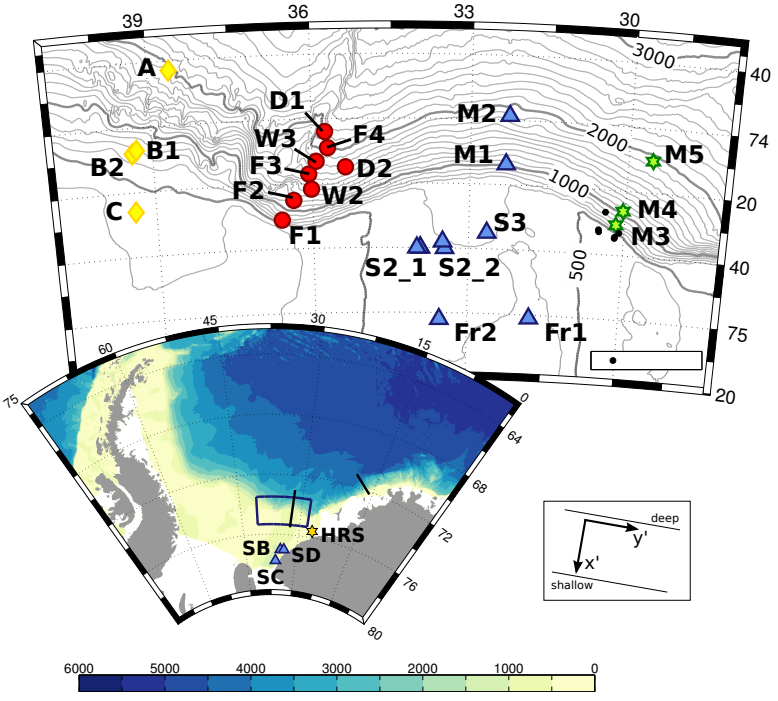

Figure 1. Map of the Weddell Sea (bathymetry from The GEBCO_2014 Grid, version 20150318, http://www.gebco.net) and locations of moorings in the study area (colours and shapes according to their location west, along the ridge, at and in the Filchner Depression, or east on the continental slope). S2_1 and S2_2 show the location of mooring S2 prior to and after 2000. The study area is also the area the sea ice concentration has been averaged over. The yellow star marks Halley Research Station (HRS), while the two black lines indicate cross-slope sections used for the bathymetry test in the numerical code and to derive diurnal tidal KE from the tidal model CATS. The inset in the lower right corner illustrates the rotation of the coordinate system.

Ocean Sci. Discuss., doi:10.5194/os-2016-36, 2016
Manuscript under review for journal Ocean Sci.
Published: 14 June 2016

Ocean Science
Discussions
Open Access
EGU

Table 1. Name, recording year, location in degrees and minutes, bottom depth, number of recording days, depths of current meters or ADCPs (in format "first level:depth increment:last level") in metres above bottom (m.a.b.) and angle β for the clockwise rotation of the coordinate system for all moorings used in this study. For some moorings located on the flat shelf or close to varying bathymetry (i.e. at the ridge), the rotation angles have increased uncertainty (marked with an asterisk). More details on the moorings can be found in Foldvik et al. (2004) and references therein, as well as in Jensen et al. (2013) and Darelius et al. (2016).

Mooring	Year	Latitude	Longitude	Depth (m)	Recording days	Instrument depth (m.a.b.)	β
B1	1968	-74 07	-39 18	657	265	23	122
B2	1968	-74 08	-39 23	663	460	23	122
S2-1977	1977	-74 40	-33 56	558	411, 257	25, 100	-10*
C	1977	-74 26	-39 24	475	630, 631	25, 125	127
A	1978	-73 43	-38 36	1939	65, 440	25, 125	123
S2-1985	1985	-74 40	-33 56	545	371, 283, 258	25, 100, 190	-10*
D1	1985	-74 04	-35 45	2100	352	25, 100	13*
D2	1985	-74 15	-35 22	1800	281, 52	25, 100	70*
S2-1987	1987	-74 40	-34 00	558	352, 407	25, 100	-10*
S3	1992	-74 35	-32 39	659	165, 356	70, 170	-10*
Fr1	1995	-75 01	-31 46	610	691, 837, 828, 828	20, 126, 232, 353	50*
Fr2	1995	-75 02	-33 33	574	683, 837, 829, 829	20, 126, 232, 383	25
F1	1998	-74 31	-36 36	647	327, 277, 393	10, 56, 207	124
F2	1998	-74 25	-36 22	1180	309, 390, 326, 348	10, 56, 202, 433	106
F3	1998	-74 17	-36 04	1637	395	56, 413	94
F4	1998	-74 09	-35 42	1984	376, 390, 332	10, 56, 207	90
S2-2003	2003	-74 40	-33 28	596	421	25, 100	-10*
M1	2009	-74 13	-32 19	967	365	25, 46	110
M2	2009	-73 58	-32 16	1898	364	19, 78:4:150	110
M3	2009	-74 30	-30 09	725	361	25, 123:4:1993, 10:5:505	110
M4	2009	-74 26	-30 02	1051	361	25, 442:16:986	110
M5	2009	-74 10	-29 32	1917	361, 336	26, 55:16:391	110
S2-2010	2010	-74 38	-33 30	612	363	25, 104, 176	-10*
W2	2010	-74 23	-36 01	1411	361, 344, 302, 318	25, 84, 194:4:234, 289:4:389	94
W3	2010	-74 13	-35 55	1488	363, 363, 91, 304	25, 93, 163:2:209, 216:4:272	97
SB	2013	-77 00	-34 28	705	371	51:8:395	37
SC	2013	-77 45	-36 09	700	376	26:4:214	28
SD	2013	-77 00	-34 03	505	371	19:4:119	37
SE	2013	-77 01	-34 14	590	196	175	37

Ocean Sci. Discuss., doi:10.5194/os-2016-36, 2016
Manuscript under review for journal Ocean Sci.
Published: 14 June 2016

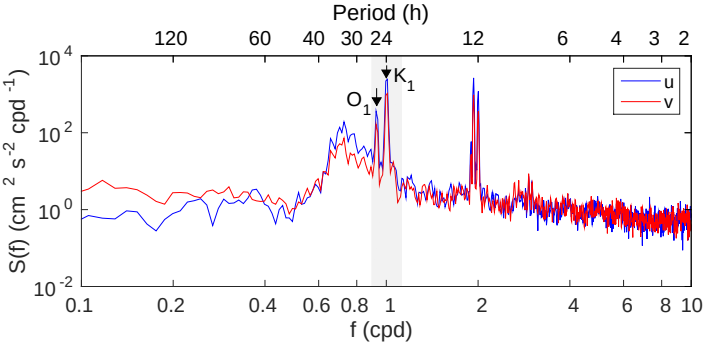

Figure 2. Power spectral density of depth-averaged, rotated u- and v-velocity components at mooring M3. The diurnal tidal frequency band around one cycle per day (cpd) is marked in grey; black arrows indicate frequencies of the K_1 and O_1 tidal constituents.

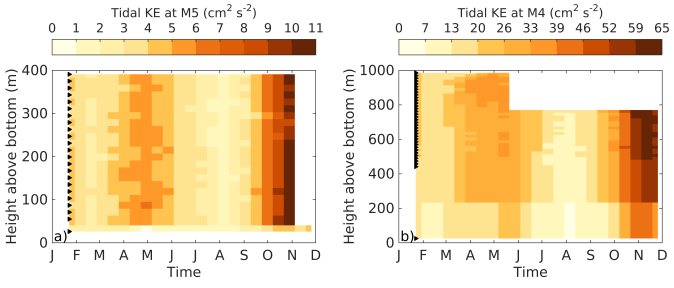

Figure 3. Diurnal tidal KE over time and depth at a) mooring M5 and b) mooring M4 on the continental slope. Black triangles mark the depths of individual measurements. Note the different scale for diurnal tidal KE and vertical axis in a) and b).

Table 2. Parameters of the reference stratification profile and corresponding ranges of change in the sensitivity test (SM: surface magnitude, SSM: subsurface magnitude, SSD: subsurface depth, DM: deep magnitude). For case DM, the average (av.) is given in addition to the range of values in the profile section.

	SM, 10^{-5} s^{-2}	SSM, 10^{-5} s^{-2}	SSD, m; model level	DM, 10^{-7} s^{-2}
reference stratification	3.20	0.17	640; 5	1.99–4.42; av.: 2.92
sensitivity test	0.07–4.05	0.04–2.78	320–960; 3–7	1–30

Ocean Sci. Discuss., doi:10.5194/os-2016-36, 2016
Manuscript under review for journal Ocean Sci.
Published: 14 June 2016

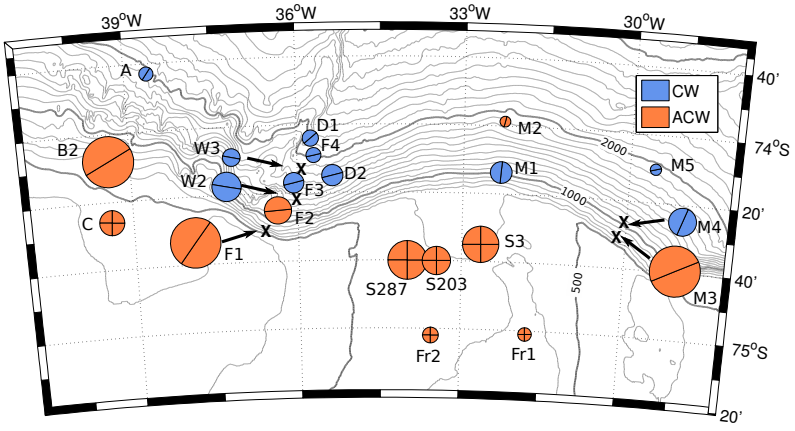

Figure 4. The area of the circles on the map is proportional to the square root of the maximum of depth-averaged, diurnal tidal KE reached in austral summer. Blue circles indicate a clockwise (CW) rotation of tidal currents at the K_1 frequency, red circles an anticlockwise (ACW) rotation, as inferred from harmonic analysis. The line through the circles indicates the orientation of the major axis (i.e. strongest tidal current). Tidal current ellipses with an aspect ratio (semi-minor/semi-major axis) of more than 0.8, i.e. close to circular, are marked with two crossing lines instead of a single line. At the location of mooring S2 with five years of measurements, the data for the deployment years 1987 (S287) and 2003 (S203) are presented. Some circles are displaced from their actual mooring locations (marked with "X") for legibility.

Ocean Sci. Discuss., doi:10.5194/os-2016-36, 2016
Manuscript under review for journal Ocean Sci.
Published: 14 June 2016

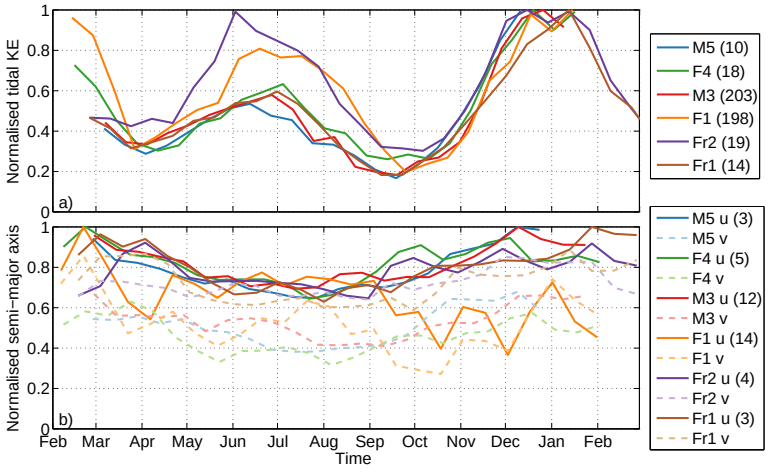

Figure 5. a) Time series of normalised diurnal tidal KE at moorings M5 and F4 (deeper continental slope), M3 and F1 (shelf break) and the first year of record at Fr2 and Fr1 (shelf). At M5, KE is only calculated until the ADCP stops measuring (see Table 1). The maximum diurnal tidal KE values in $cm^2\ s^{-2}$ are given in parentheses in the legend. b) Time series of normalised magnitudes of semi-major axes of tidal currents at the K_1 frequency (separated from P_1) at the same moorings, as obtained from harmonic analysis (see Section 2). The u-components are shown by solid lines, the respective v-components by broken, lighter-coloured lines. The major axes obtained from T_TIDE are normalised with the maximum u-velocity at the respective mooring. At M5, major axes are only calculated until the ADCP stops measuring (see Table 1). The magnitudes in $cm\ s^{-1}$ for the u-components of the semi-major axes are given in parentheses in the legend.

Ocean Sci. Discuss., doi:10.5194/os-2016-36, 2016
Manuscript under review for journal Ocean Sci.
Published: 14 June 2016

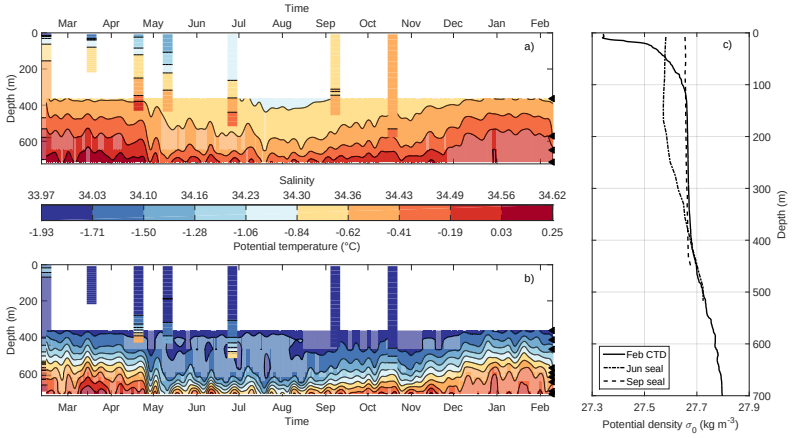

Figure 6. Hovmöller diagrams for a) salinity and b) temperature. The continuous records below approximately 350 m depth are the hydrographic time series of moored instruments at M3, acquired in 2009 (see Table 1). The mooring data have been low-pass filtered by applying a fourth order Butterworth filter removing variability at shorter periods than the cut-off period of 168 h (one week). Black triangles mark the depths of individual measurements. CTD profiles from ship (from the deployment cruise of mooring M3 in 2009, first profile) and seals (obtained in 2011 from within approximately 10 km distance to mooring M3, see Fig. 1) complement the mooring records. The width of the profiles is arbitrarily set to one week for clarity. Panel c) shows the seasonal development of potential density based on three of the temperature and salinity profiles near mooring M3.

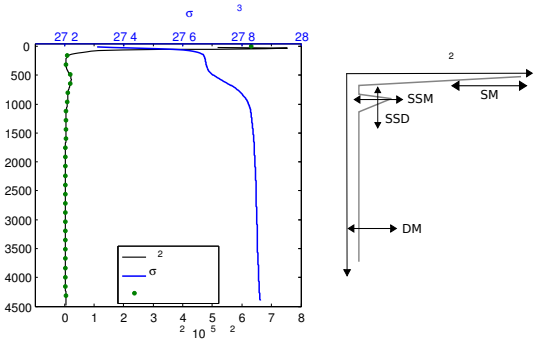

Figure 7. a) Profiles of potential density (blue line) and resulting stratification ("reference stratification", black line) from historic CTD data obtained in January and February in the area of moorings M1 to M5, merged with profiles from the deeper Weddell Sea at depth. Green markers indicate the vertical levels of the numerical code. b) Illustration of reference stratification (grey line). Arrows indicate direction (but not magnitude) of changes in sensitivity tests (SM: surface magnitude, SSM: subsurface magnitude, SSD: subsurface depth, DM: deep magnitude).

Ocean Sci. Discuss., doi:10.5194/os-2016-36, 2016
Manuscript under review for journal Ocean Sci.
Published: 14 June 2016

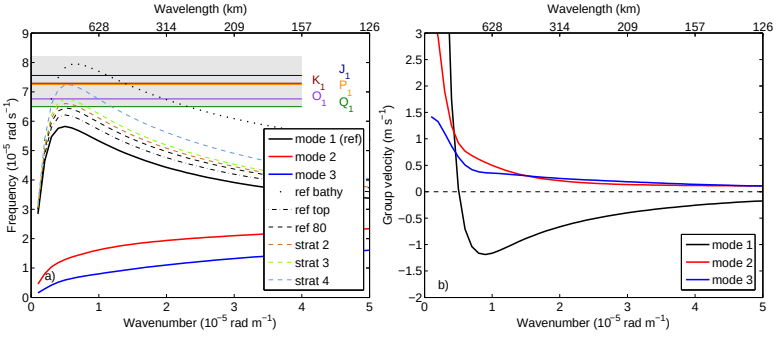

Figure 8. a) Dispersion curves for CTWs of modes 1–3 using the reference stratification (thick lines). In addition, the dispersion curves for mode 1 CTWs for the bathymetry east of the study area (ref bathy), differently inferred surface N^2 values for the reference stratification (top value profile, ref top, and average upper 80 m, ref 80) and three other stratification profiles are shown. Stratification profiles 2–4 are representative for regions in the study area with increasing distance west of the reference stratification and inferred similarly. The diurnal tidal band is shaded in light grey with the most important diurnal frequencies marked by coloured lines. b) Group velocities for CTWs of modes 1–3 using the reference stratification. Zero group velocity is indicated by a dashed line.

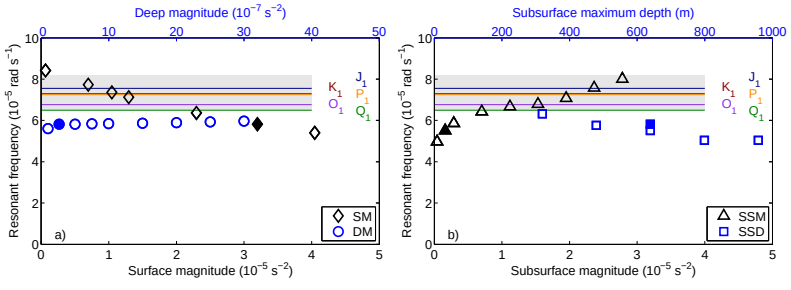

Figure 9. Sensitivity test for changing stratification. a) The surface magnitude (SM) and deep magnitude (DM) are varied. b) The subsurface magnitude (SSM) and its depth (SSD) are varied. Results from the reference stratification profile are indicated by filled markers. For case SSD, the shape of SSM in the profile is simplified (open marker below filled marker) and then varied in depth. The diurnal tidal band is shaded in light grey with the most important diurnal frequencies marked by coloured lines.

Ocean Sci. Discuss., doi:10.5194/os-2016-36, 2016
Manuscript under review for journal Ocean Sci.
Published: 14 June 2016

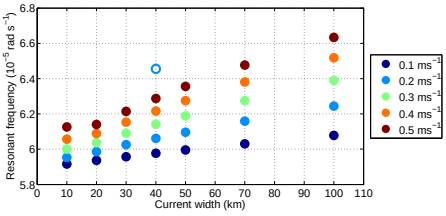

Figure 10. Sensitivity test for changing the width and strength of the slope current. Additionally, an example for the RF of a less barotropic (i.e. surface-enhanced) current is shown by the open blue marker. RF$\approx 5.8 \cdot 10^{-5}$ rad s^{-1} corresponds to the result of the numerical code for the reference stratification without added current (see Fig. 8).

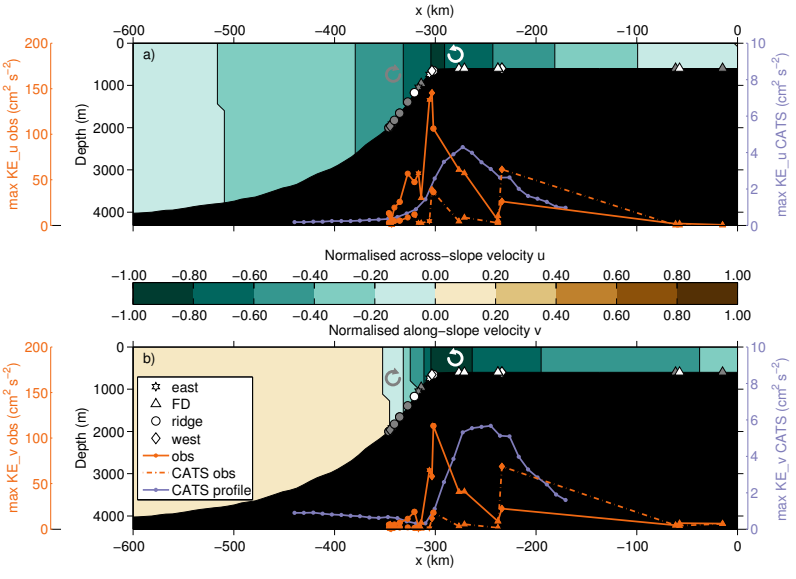

Figure 11. Normalised arbitrary along-slope perturbation velocity from the numerical code (background colours) at the wavenumber of the RF for reference stratification. Moorings within the modelled domain are indicated by markers whose shapes correspond to the geographic locations (west, ridge, Filchner Depression, east) as in Fig. 1. Markers filled in grey (white) indicate a clockwise (anticlockwise) rotational sense of the diurnal tidal currents. For each mooring location, diurnal tidal KE for austral summer is shown, both from observations (solid orange line) and derived from CATS (broken orange line). Diurnal tidal KE predicted from the CATS run along the cross-shelf section through the locations of moorings M1 and M2 (see Fig. 1 for location) is shown as purple line with markers indicating locations of predicted currents. Panel a) shows u-velocity, b) v-velocity; the legend is shared.

Ocean Sci. Discuss., doi:10.5194/os-2016-36, 2016
Manuscript under review for journal Ocean Sci.
Published: 14 June 2016

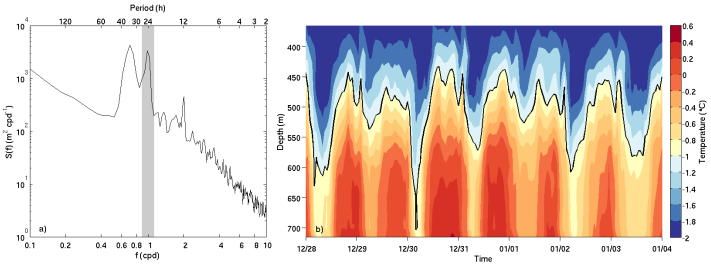

Figure 12. a) Power spectral density of the height above the bottom of the -1° C isotherm indicating the transition between WW and WDW at M3. The diurnal tidal frequency band is marked in grey. b) Hovmöller diagram of low-passed filtered temperature at mooring M3 from 28 December to 4 January. The -1° C isotherm is shown by a black line.

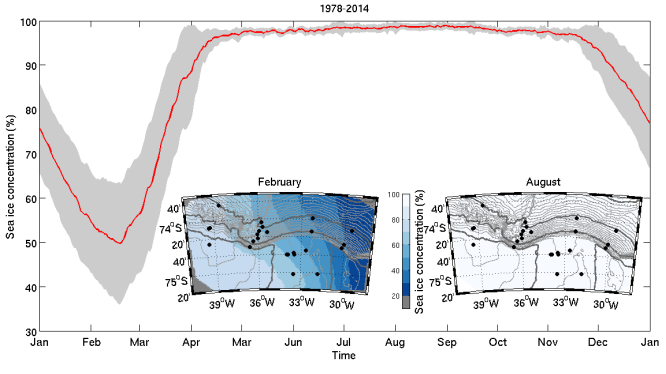

Figure 13. Sea ice concentration averaged over the study area and the period 1978-2014 (red line) with standard deviation (grey). Insets show maps of mean sea ice concentrations in February and August; isobaths and mooring locations (black dots) are as in Figure 1.